Error Propagation in Directly Georeferenced Terrestrial Laser Scanner Point Clouds for Cultural Heritage Recording

Derek D. LICHTI and Stuart J. GORDON, Australia

Key words: key words, theme, etc.

SUMMARY

Cultural heritage recording is a prime application for terrestrial laser scanners due to the high spatial resolution, high accuracy and fast data capture rates offered by this technology. To date, insufficient attention has been given to the many error sources contributing to the uncertainty of scanner datasets. A full error budget is derived for directly georeferenced terrestrial laser scanner networks that considers both relevant error sources fundamental to surveying and those unique to sampled laser scanner systems. In the case of the latter, new probabilistic models are proposed for angular positional uncertainty due to laser beamwidth and target centroid pointing. Analysis of a cultural heritage recording project in Ayutthaya, Thailand, highlights the disparity between 'expected' precision and the more realistic precision indicated by the error budget, to which the laser beamwidth is demonstrated to be a significant contributor.

Error Propagation in Directly Georeferenced Terrestrial Laser Scanner Point Clouds for Cultural Heritage Recording

Derek D. LICHTI and Stuart J. GORDON, Australia

1. INTRODUCTION

Terrestrial laser scanners (TLSs) have found application to many measurement tasks, particularly for engineering projects and cultural heritage recording. Their high resolution, accurate and rapid point cloud capture capabilities allow cost effective production of as-built engineering models and digital documentation of cultural heritage features. Though TLSs have been readily adopted, insufficient attention has been given to the precision of the point clouds they produce. It would seem that the stunning appearance of the derived models, and even that of the raw point clouds themselves, has overshadowed the fundamental issue of error propagation.

This paper presents an analysis of random error sources for directly georeferenced TLS point clouds. By direct georeferencing, we mean levelling, optical centring and orientation via telescope. An error budget for resection or indirectly georeferenced scanners is presented in Gordon and Lichti (2004). The prime motivation for this investigation is to provide rigorous, quantitative measures that will allow laser scanner users to understand the limitations of a particular instrument and the data cloud it produces and facilitate pre-analysis during project planning. Misunderstanding of an instrument's capabilities and sub-optimal scanner network design can lead to project specifications and desires not being met.

Many of the contributing error sources are common to the surveying field, as might be expected given the nature of the georeferencing method. A significant component in the random error budget that is not considered in standard surveying error analysis—but should be for both scanners and reflectorless total stations—is the uncertainty in the angular location of a range measurement due to the finite laser beam diameter. The presence of this error in airborne laser scanning is acknowledged (Huising and Pereira 1998) but not quantified, perhaps since it may be relatively small compared to other sources such as kinematic georeferencing errors. It is, however, a serious issue for TLS surveying, particularly for mapping intricate details on features such as historic building façades. A probabilistic model for this uncertainty is derived and its contribution to the budget analysed. Furthermore, a model is proposed for centroid-derived target pointing, which is an alternative to optical pointing for direct scanner orientation and is commonplace for georeferencing by three-dimensional resection. A heritage-recording case study undertaken at the UNESCO World Heritage listed Wat Mahathat site in Ayutthaya, Thailand, is presented in which the budget is first analysed in terms of its components, then holistically for the entire site.

2. CULTURAL HERITAGE RECORDING BY TLS

One of the earliest and most prolific uses of TLS has been in the field of cultural heritage documentation. This may entail any task from the digital preservation of historic and culturally significant structures to mapping archaeological dig sites. Laser scanning for cultural heritage recording is increasing in popularity, as indicated by moves to create standards for metric TLS surveys (Barber et al. 2003). Though the accuracy requirements for a cultural heritage survey may not usually be as demanding as for, say, engineering projects, a heritage survey requires the highest level of imaging resolution so that intricate features can be faithfully mapped.

There are numerous scoping papers in which authors discuss the potential of TLS for cultural heritage recording and report research findings (Barber et al. 2001; Boehler et al. 2001; Bornaz et al. 2003; Fangi et al. 2001). Caprioli and Scognamiglio (2003) investigate integrating (analogue and digital) photogrammetry and TLS for preparing 'metric documentation' of heritage monuments. Wehr and Wiedemann (2001) investigate the fusion of photogrammetric imagery with TLS data for increasing the intelligence of the 3D datasets. Guidi et al. (2002) describe the integration of multiple sensors (steel band, digital level, digital camera and pulsed- and triangulation-method laser scanners) for digitally recording scenes at archaeological dig sites. Afshar et al. (2002) describe scanning the ancient city of Persepolis (Iran) to produce site plans (scales of 1:200 and 1:500) and provide a medium to make off-line measurements (e.g. co-ordinates and lengths).

3. TLS OPERATION

Regardless of application, the logical starting point for constructing the error budget is TLS operation, which is briefly reviewed here. The fundamental observable of a TLS system is range. Several techniques for laser range measurement exist, including triangulation, phase difference and the time-of-flight or pulse method. Amann et al. (2001) provide a comprehensive overview of rangefinding methods. In the case of the pulse method, which is the method used by the TLSs described in this paper, range is derived from the two-way propagation time of a brief pulse of laser radiation.

Laser scanners provide a sampled representation of a scene by making a series of range measurements in uniform angular increments in both horizontal and vertical planes. Rotating mirrors, nodding mirrors, rotating-head mechanisms or a combination of these deflect the laser beam to create the uniform sampling lattice. Three-dimensional Cartesian co-ordinates for each measured point are derived from the basic measurements of range, ρ, horizontal direction, θ, and elevation (vertical) angle, α. It is important to note that these co-ordinates are referenced to the instrument's internally defined system, (x, y, z), which makes georeferencing into an external co-ordinate system, (X, Y, Z), necessary. Figure 1 illustrates the observables and related co-ordinate systems in the context of the direct scanner georeferencing.

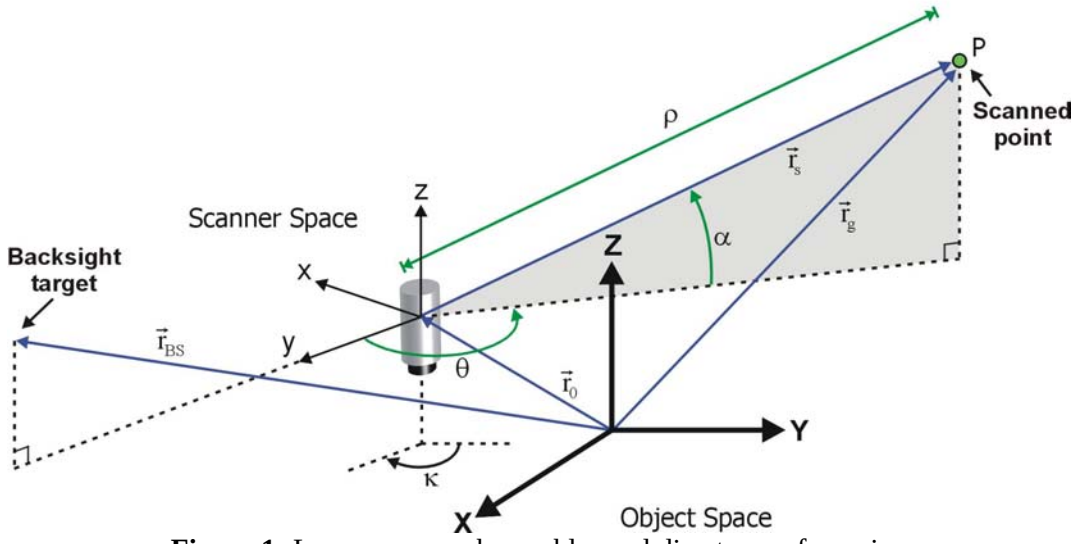

Figure 1: Laser scanner observables and direct georeferencing

3.1 Review of Commercially Available Direct-Georeference TLSs

Most TLSs enable cloud georeferencing using 3D resection. However, it is probable that TLS technology may evolve closer to traditional total station sensors. Prior to investigating the error sources, it is prudent to first review some commercially available directly-georeferenced instruments. The Leica HDS3000, successor to the HDS2500 (formerly known as the Cyra Cyrax 2500), can be optically centred over a known point and levelled. Unlike a total station, however, it is not optically oriented toward a known point but uses high resolution scanning and a centroid estimation algorithm to 'observe' the centre of the backsight target.

Although georeferencing by resection is advocated by the manufacturer, the Riegl series of laser mirror scanner (LMS) products (e.g. LMS-Z420i, LMS-Z210i) also can be directly oriented. The telescope bundled with the instruments has low magnification (3x) and is not supplied as a standard accessory but as an optional item. The I-SiTE 4400 is the closest TLS to a conventional total station (at time of writing). It offers a level bubble and optical plummet and backsighting is done via a 16x telescope. Similar to many modern total stations, the telescope pointing is facilitated by motors. Callidus permit orientation using an internal compass (±3°), but given such low precision it may be more pragmatic to employ the centroid method.

3.2 Laser Beamwidth

One of the salient properties of a scanner that strongly influences both point cloud resolution and positional uncertainty is the laser beamwidth. An emitted laser beam expands in radius, w, from a minimum called the beam waist, w_0, according to (Weichel, 1990)

$$w(\rho_w) = w_0\sqrt{1+\left(\frac{\lambda\rho_w}{\pi w_0^2}\right)^2} \tag{1}$$

where ρ_w is range relative to the beam waist location. The expansion is linear for large ranges, so divergence is often specified in terms of initial diameter plus a linear expansion factor, which may be expressed in mrad, or just the expansion factor itself. Though several diameter definitions exist, the most common definition is e^{-2}, which encircles 86% of the total beam power within the Gaussian irradiance distribution (Marshall 1985). Of those TLSs mentioned, the Leica HDS3000 possesses a spot size of 6mm at 50m, 13mm at 50m for the Riegl LMS-Z420i, 120mm at 50m for the I-SiTE 4400 and for the LMS-Z210i, approximately 150mm at 50m.

The practical ramification of a finite laser beamwidth is inherent uncertainty in the angular location of the point to which the range measurement is made. The *apparent* location of the range observation is along the centreline of the emitted beam. However, the *actual* point location cannot be predicted since it could lie anywhere within the projected beam footprint. Figure 2 illustrates the effect. Pictured is a high-resolution Cyra Cyrax 2500 (now the Leica HDS 2500) scan of 0.5mm diameter, 2m long, tensioned vertical plumb line. Visible are twelve point-loci, 2mm – 4mm in length, which cross the best-fit line (as determined by least-squares geometric form fitting) at an acute angle of approximately 0.4° (note that the axes differ in scale). The point bands result from the approximately 6mm diameter laser beam illuminating the plumb line at several sample locations where sufficient energy was backscattered to register a range measurement. Boehler et al. (2001) refer to this effect as 'parallax'.

Though the plumb line's actual location and, thus, the angular displacement errors, are somewhat clear from the geometric form fitting, the error magnitude is unpredictable since the location and shape of scanned objects are generally not known *a priori*. A probabilistic model is therefore required to quantify the anticipated level of uncertainty. Assuming a laser beam of circular cross-section having diameter δ (in angular units) and that the probability governing the angular position (θ,α), of the range measurement is uniform within the beam's cross-section, then the associated probability density function for beamwidth uncertainty is given by

$$p_b(\theta,\alpha) = \begin{cases} \dfrac{4}{\pi\delta^2} & \alpha^2+\theta^2 < \dfrac{\delta^2}{4} \\ 0 & \alpha^2+\theta^2 > \dfrac{\delta^2}{4} \end{cases} \tag{2}$$

The standard deviation for beamwidth uncertainty is obtained from the root of either second moment since the density function is isotropic and its mean in both dimensions is zero, i.e.

$$\sigma_b = \pm\sqrt{\int_{-\infty}^{\infty}\int_{-\infty}^{\infty}\alpha^2 p_b(\theta,\alpha)\,d\alpha\,d\theta} = \pm\frac{\delta}{4} \qquad (3)$$

Thus, beamwidth uncertainty is, rather elegantly, equal to one-quarter of the laser beam diameter. The question of the significance of this error source must be answered in an analysis of all contributing error sources, as will be demonstrated shortly.

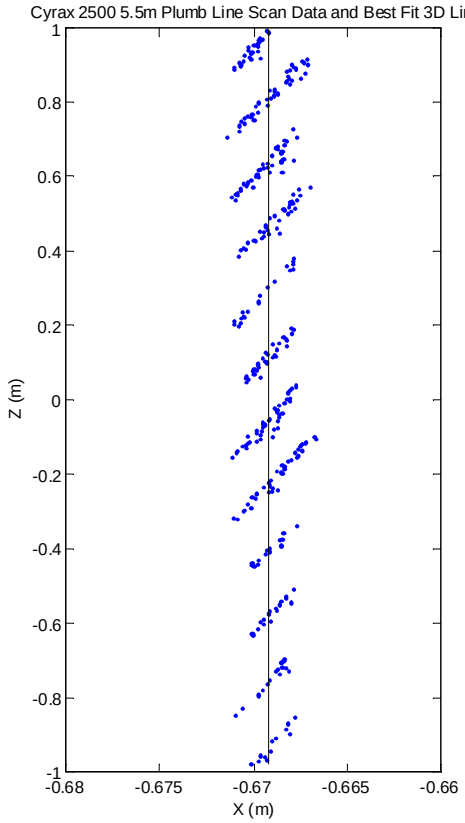

Figure 2: Cyrax 2500 plumb line point cloud and best-fit line

4. DIRECT GEOREFERENCING ERROR BUDGET

In composing the error budget for the points in a scanned point cloud, one must consider the contribution of all random error sources. These include internal sources (e.g., noise in the observations, beamwidth uncertainty) and external sources (e.g., the survey points used for registration and instrument setup errors). Propagation of the random errors through the functional model for scanner point positioning produces a 3x3 point covariance matrix that contains all positional precision information. It is important to recall that point positions are uniquely determined by radiation from the scanner, so the redundancy of the survey network needed for registration does not extend to the point cloud.

The transformation of a point from scanner space to an external system—object space—is given by the vector equation

$$\vec{r}_g = \vec{r}_0 + R_3(\kappa)\vec{r}_s \tag{4}$$

where

$$\begin{aligned}\vec{r}_s &= \begin{bmatrix}\rho\cos\alpha\cos\theta & \rho\cos\alpha\sin\theta & \rho\sin\alpha\end{bmatrix}^T \\ &= \begin{bmatrix}x & y & z\end{bmatrix}_s^T\end{aligned} \tag{5}$$

is the vector of scanner space (s) co-ordinates,

$$\vec{r}_g = \begin{bmatrix}X & Y & Z\end{bmatrix}_g^T \tag{6}$$

is the vector of georeferenced object space (g) co-ordinates,

$$\vec{r}_0 = \begin{bmatrix}X & Y & Z\end{bmatrix}_0^T \tag{7}$$

is the vector of object space, setup station (0) co-ordinates, κ is the derived azimuth from the setup station to the backsight station and

$$R_3(\kappa) = \begin{bmatrix}\cos\kappa & \sin\kappa & 0 \\ -\sin\kappa & \cos\kappa & 0 \\ 0 & 0 & 1\end{bmatrix}. \tag{8}$$

For directly georeferenced point clouds, contributing error sources include: (i) the survey stations used for the scanner setup and backsight target placement; (ii) instrument levelling and centring; (iii) backsight target centring; (iv) raw scanner observation noise; and (v) laser beamwidth. Considering these sources and using the variance propagation law, the 3x3 covariance matrix of a directly georeferenced, scanned point is given by

$$C_g = C_0 + \frac{\partial \vec{r}_g}{\partial \vec{r}_s}\left(C_{obs} + C_b + C_{set}\right)\frac{\partial \vec{r}_g}{\partial \vec{r}_s}^T + \frac{\partial \vec{r}_g}{\partial \kappa} C_\kappa \frac{\partial \vec{r}_g}{\partial \kappa}^T \tag{9}$$

The instrument setup station errors contribute to the point cloud position and orientation (e.g., azimuth) uncertainty, whereas the backsight station contributes only to the latter. Ideally, their 3x3 point covariance matrices obtained from a previous least-squares adjustment are isotropic (i.e., the co-ordinates are uncorrelated).

The variance of the derived azimuth is determined by propagation of the setup (0) and backsight (BS) stations' precision through the arctangent function. If horizontal co-ordinate

precision is homogeneous and isotropic and given by σ_H, and the backsight and setup stations are uncorrelated, then the derived azimuth precision is inversely proportional to the horizontal distance separating the two stations, $d_{0\text{-}BS}$

$$\sigma_A = \pm \frac{\sqrt{2}\rho\sigma_H}{d_{0-BS}} \tag{10}$$

Setup errors include instrument and target optical centring, instrument levelling and manual pointing of the orientation telescope to the backsight station. The contribution of scanner and backsight target centring to the horizontal angle error budget also is inversely proportional to the separation distance, i.e.,

$$\sigma_d = \pm \frac{\sqrt{2}\,\rho\sigma_c}{d_{0-BS}} \tag{11}$$

A centring precision of σ_c=±0.5mm/m of instrument/target height can be generally expected with optical plummets (Kuang 1996).

Instrument levelling influences both horizontal and vertical angle measurements and is a function of plate bubble sensitivity (Cooper 1982, p. 140). Its standard deviation in horizontal angle is a function of the observed elevation angle as given by

$$\sigma_{lh} = \pm\sigma_{lv}\tan\alpha \tag{12}$$

where the levelling error standard deviation in the elevation angle dimension is

$$\sigma_{lv} = \pm 0.2\nu'' \tag{13}$$

where ν'' is the level bubble sensitivity. This error may be significant if the plate bubble sensitivity is poor and if dual axis compensation is not available, as is the case with currently available TLSs.

Pointing error is inversely proportional to telescope magnification, M, but is greatly dependent on ambient atmospheric conditions (Kuang 1996, p. 9). The following is an accepted model for pointing error

$$\sigma_p = \pm \frac{60''}{M} \ . \tag{14}$$

Though the constant in the numerator may vary in the literature, the more pessimistic upper limit of 60″ is chosen here. For the 3x magnification riflescope accompanying the Riegl LMS-Z210, the error is ±20″ (1σ), or ±10mm at 100m. Though possibly negligible when

contrasted with other error sources, Equation 14 may actually be optimistic if the instrument lacks fine tangent screws to allow accurate pointing.

Instead of sighting with a telescope, a structured target centred over a known point can be densely scanned and the subsequently estimated centroid position (see Gordon and Lichti 2004) used to orient the scanner. In this case, the pointing error is governed by the (uniform) angular sampling interval, Δ, which is assumed equal in both the θ and α dimensions. If the probability that the derived centroid and the actual target centre positions coincide is uniform over the sampling interval, then the corresponding density function is given by

$$p_s(\theta,\alpha)=\begin{cases}\dfrac{1}{\Delta^2} & |\theta|<\dfrac{\Delta}{2} \quad , \quad |\alpha|<\dfrac{\Delta}{2} \\ 0 & |\theta|>\dfrac{\Delta}{2} \quad , \quad |\alpha|>\dfrac{\Delta}{2}\end{cases} \tag{15}$$

The standard deviation of centroid-derived pointing error is given by

$$\sigma_{pc}=\pm\sqrt{\int_{-\infty}^{\infty}\int_{-\infty}^{\infty}\theta^2 p_s(\theta,\alpha)\,d\alpha\,d\theta}=\pm\frac{\Delta}{2\sqrt{3}} \tag{16}$$

Though the moments of $p_s(\theta,\alpha)$ are equal in the θ and α dimensions, pointing error is only pertinent to the horizontal angle measurement for direct scanner georeferencing. For indirect georeferencing, pointing error also contributes to the elevation angle. Clearly, capturing a large number of samples over the target surface with a fine sampling interval reduces pointing error to insignificance. It is also important to note that the centroid estimate is subject to observational noise and beamwidth errors. Their contributions to the centroid uncertainty, in terms of variance, are reduced by the number of points used in the centroid computation, which is in general very large (e.g., several thousand points) if the sampling interval is small.

Combining Equations 11, 12, 13 and 14, the covariance matrix of all setup errors with optical pointing is given by

$$C_{set}=\begin{bmatrix}0 & 0 & 0\\ 0 & \sigma_{lv}^2 & 0\\ 0 & 0 & \sigma_{lh}^2+\sigma_d^2+\sigma_p^2\end{bmatrix} \tag{17}$$

whereas for centroid-derived pointing, the variance from Equation 16 is used rather than that derived from Equation 14.

In constructing the error budget, precision estimates are of course required for the observables of range, horizontal angle and elevation angle. Assuming these to be due solely

to the noise processes internal to the instrument, which may include quantisation noise and jitter (Amann et al. 2001), and that they are uncorrelated with each other, the corresponding covariance matrix is given by

$$C_{obs} = \frac{1}{m}\begin{bmatrix} \sigma_\rho^2 & 0 & 0 \\ 0 & \sigma_\alpha^2 & 0 \\ 0 & 0 & \sigma_\theta^2 \end{bmatrix} \tag{18}$$

where m is the number of averaged, repeat scans captured, a capability available with many scanner systems. Precision estimates are not always readily available from scanner manufacturers and when they are, they may be specified in terms of co-ordinate precision, modelled precision or range and angular precision, or may be (incorrectly) interchanged with accuracy and/or resolution. Regardless of which measure is provided, independent testing is of course necessary to obtain unbiased estimates.

Finally, drawing upon the model given by Equation 2, the uncertainty due to beamwidth propagates into the elevation angle and horizontal direction measurements as

$$C_{beam} = \begin{bmatrix} 0 & 0 & 0 \\ 0 & \sigma_b^2 & 0 \\ 0 & 0 & \sigma_b^2 \end{bmatrix}. \tag{19}$$

5. HERITAGE RECORDING CASE STUDY

5.1 Wat Mahathat, Ayutthaya

The city of Ayutthaya, Thailand, is located approximately 85km north of Bangkok. An ancient capital of Siam, it holds UNESCO World Heritage status for the many culturally significant Wats in the city and its environs. One such site, Wat Mahathat, is pictured in Figure 3. It was scanned over five days in February 2003 in order to create a three-dimensional virtual model to support education and historical interpretation of the site. Dilapidation of the red brick and mortar structures caused by ancient invading armies, vandalism and natural weathering is severe. This coupled with many occlusions made obtaining complete coverage of the site a challenge. Figure 4 is a schematic site map. The portion of Wat Mahathat that was scanned is contained within an 80m x 80m courtyard surrounded by a 3m high wall. The main area of interest was the 45m x 45m cluster of structures (chedi and prangs) around the base of the remains of the main prang, which rises some 18 m above the courtyard.

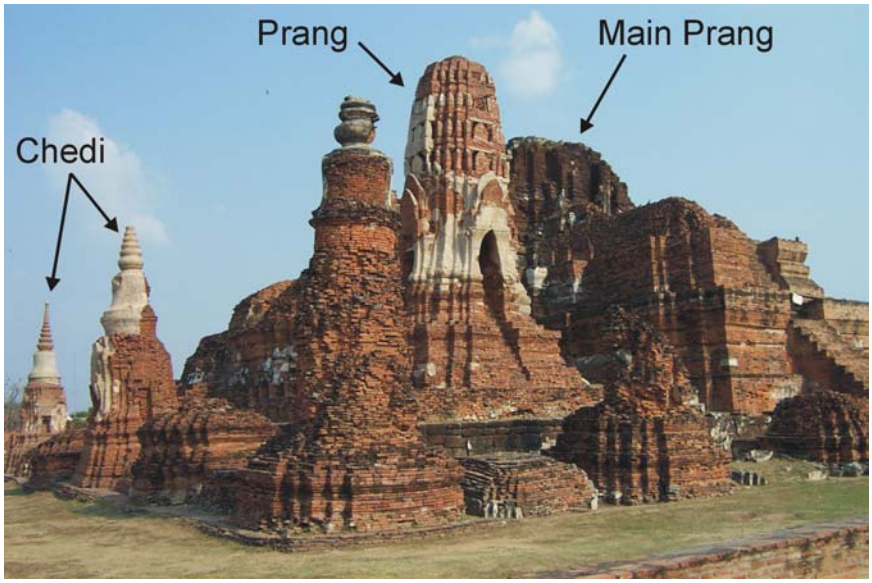

Figure 3: Wat Mahathat, Ayutthaya, Thailand

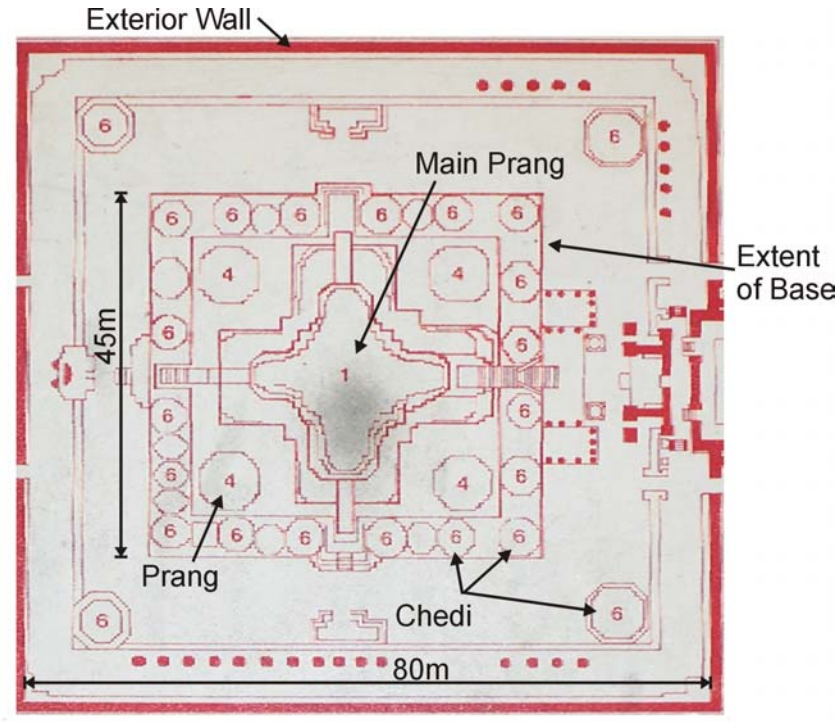

Figure 4: Plan of the Wat Mahathat site

5.2 Instrumentation

A Riegl LMS-Z210 scanner was used for the recording, but some of its components were upgraded in-house using survey quality equipment. The stock plate level bubble was replaced with one from a Wild T1A theodolite, the standard Riegl 3x magnification telescope was replaced with a 30x scope, also from a T1A, and a tribrach with optical plummet was added.

The authors' past experiences with this scanner ruled out indirect georeferencing due to its coarse sampling capabilities and broad beamwidth (3 mrad diametric divergence).

A Trimble 5600-series DR200+ total station was used to establish a 3D survey network within a local Cartesian co-ordinate system to control the laser scanning. Heights were determined by reciprocal trigonometric levelling, which was sufficient for the purposes of this recording project. A strong, redundant network was designed within the occlusion constraints of the various chedi and prangs. A 3D inner-constraints least-squares adjustment was performed and Baarda's data snooping and iterative variance component estimation were applied to optimise the solution. Station precision was very homogeneous and the largest 95% confidence ellipse semi-major axis, height error bar and ellipsoid semi-major axis were ±2.7mm, ±2.6mm and ±3.7mm, respectively. Setup and backsight station covariance matrices for the error propagation were extracted from the full estimated parameter covariance matrix.

5.3 Error Analysis for Simulated Data

Prior to analysing the error distribution of the Ayutthaya scanner data, it is prudent to first examine the contributions of each error budget component and the overall effect on the resulting co-ordinates. The relevant parameters for this simulation are presented in Table 1. Most have been obtained from manufacturer's specifications (Riegl 2001), except for the covariance matrix of the setup station, backsight distance and instrument and target heights. The dominant angular error-sources are beamwidth error (±155″) followed by angular observation nose (vertical: ±130″; horizontal: ±65″), while the others are on the order of a few arcseconds.

To assess propagated co-ordinate precision, the root of the maximum eigenvalue, $\sqrt{\lambda_{max}}$, of C_g—the confidence ellipsoid semi-major axis—scaled to 95% confidence is used. Presented in Figure 5 are the standard deviations in each co-ordinate dimension and the ellipsoid semi-major axis plotted as a function of horizontal distance from scanner for elevation angles of 0° and 40°. The X dimension nominally corresponds to range, Z to elevation and Y is orthogonal to both. The maximum distance of 80 m corresponds to Ayutthaya project site extents. At 0°, the error sources decouple in the cardinal co-ordinate directions, so error growth is linear, whereas the range and height components grow quadratically at the 40° elevation angle. Clearly, the angular components grow more rapidly than the range error, which causes the discontinuity in the ellipsoid semi-major axis between 20m and 25m distance. Note that the ellipsoid semi-major axis error measure reaches nearly ±300mm at 95% at 80m distance. Though only a simulation, it gives a clear indication of the magnitude of uncertainty that may be encountered.

Table 1: Error Propagation Parameters for the Riegl LMS-Z210

Parameter	Numerical Value
σ_ρ	$\pm\sqrt{(0.025)^2 + (20\cdot 10^{-6}\rho)^2}$ m
σ_α	±0.036° (±130″)
σ_θ	±0.018° (±65″)
ν	30″
M	30
C_0	$(0.001)^2$ I m^2
δ	3mrad (619″)
σ_b	±155″
$d_{0\text{-}BS}$	80m
IH, TH	1.5m

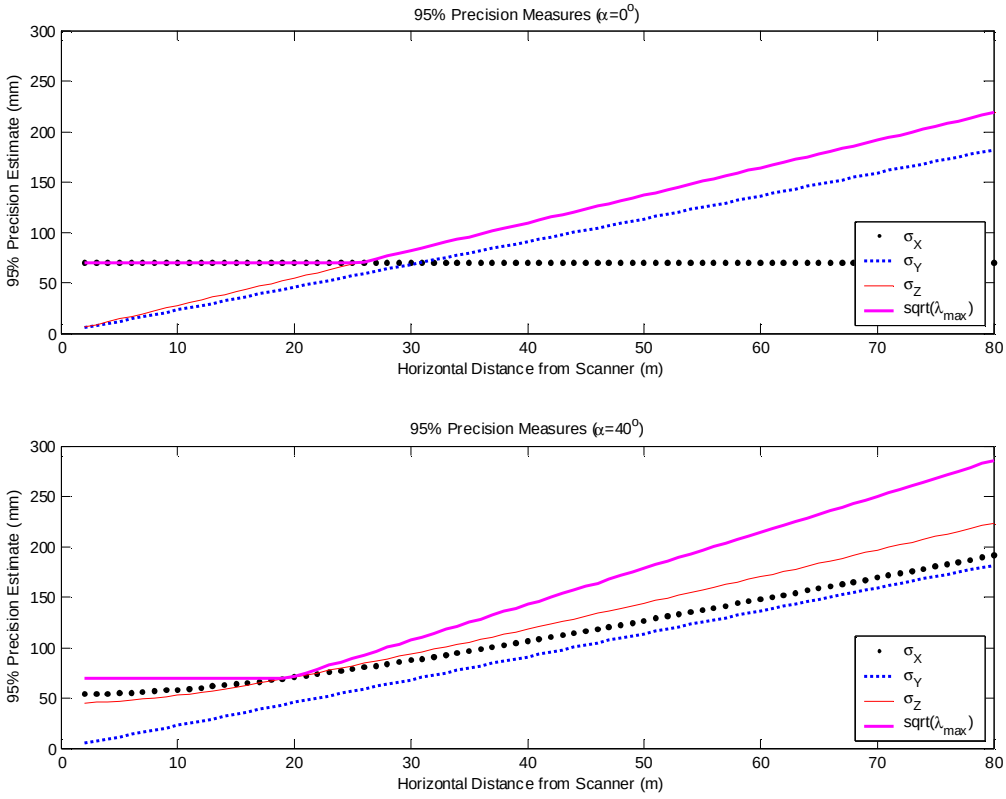

Figure 5: Simulated error propagation results (α=0° and 40°; 95% confidence)

5.4 Error Analysis for the Wat Mahathat Site

Full error propagation was performed for 525,674 points on a 100mm x 100mm grid within the courtyard area of the Wat Mahathat point cloud. The fine grid interval was chosen to ensure that any discontinuities in the error surface due to the many occlusions by structures on the site were highlighted. The root of the maximum eigenvalue of C_g scaled to 95% was

again used for assessment and ranged between ±70mm ±195mm, though 73% of all points fell below the RMS of ±82mm and more than 90% were less than ±100mm. Point precision is lower than what might be expected from the advertised—and often emphasised—range observation precision of ≈±50mm (at 95% confidence), largely due to the beamwidth uncertainty.

Figure 6 is a contour-plot of the smoothed (using a 9x9 moving average filter for display clarity only) 95% error surface of the point cloud. The error is homogeneous throughout most of site with notable exceptions in the centre atop the main prang and at the courtyard extents where georeferenced co-ordinate standard deviations exceeded ±140mm. Other minor inhomogeneities occur in areas that could not be scanned from the nearest instrument location due to occlusions but were captured from more distant stations. Though the attained precision is more than adequate for this particular heritage-recording project, this demonstration shows that complete error modelling is necessary to rigorously quantify data quality. It is also likely that an inexperienced operator, perhaps lacking a geomatics background and unaware of the intricacies of error propagation, would quote the advertised co-ordinate precision (or, range precision, or whatever metric appears on the TLS sales brochure) as a quality indicator for the entire site.

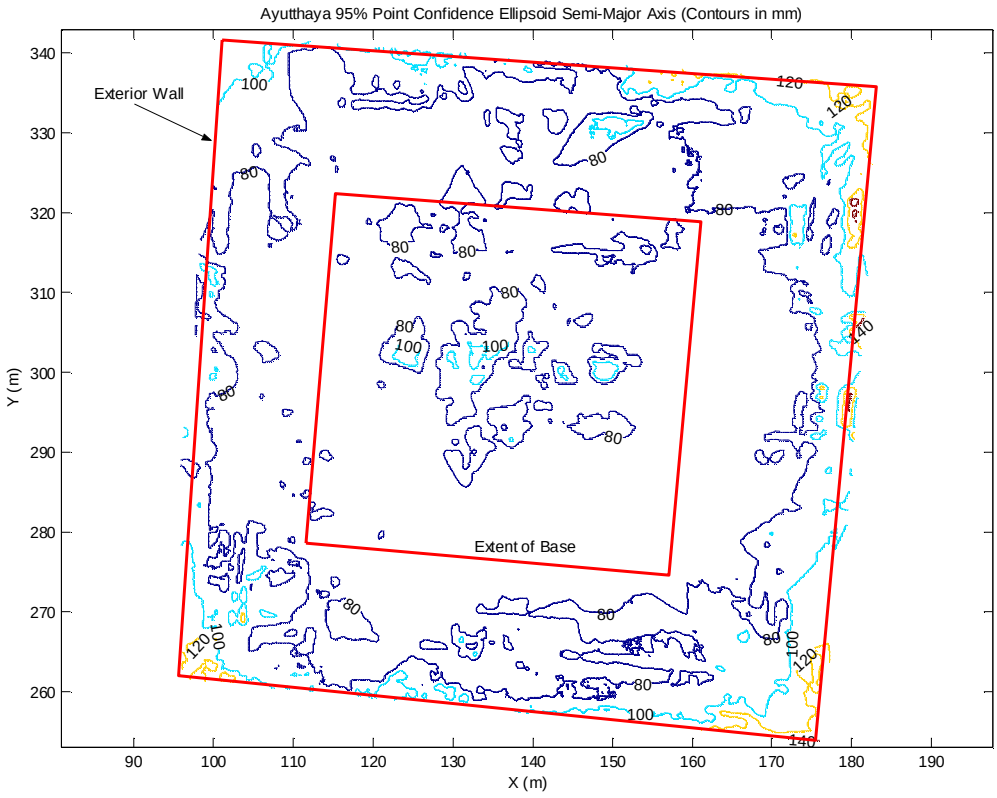

Figure 6: Ayutthaya 95% error surface contours (contours in mm)

6. CONCLUSIONS

A full error budget for directly georeferenced terrestrial laser scanner networks has been compiled. New probabilistic models for angular positional uncertainty due to finite laser beamwidth and centroid pointing have been proposed and the former was demonstrated to be a significant error source. Though many of the error sources reviewed are fundamental to elementary surveying, the subject of error propagation has seemingly been a casualty of the rapid emergence of the very impressive TLS technology. This paper has attempted to revisit error propagation specifically for terrestrial laser scanners in order for users to set realistic expectations for TLS surveys.

Cultural heritage recording projects such as Ayutthaya are prime applications for TLS since unprecedented levels of detail can be captured with relative ease in a short time span. The purpose of profiling this project was to again highlight the propagation of all error sources. The analysis indicated that estimated precision of all points in the network was poorer than the advertised range precision—which is often taken to be gospel—for the scanner in question. Though the precision requirements for this project were not demanding, it is recommended that similar analysis be conducted for any such project in order that realistic project specifications be set and fulfilled.

REFERENCES

Afshar, M., Borourmand, M., and Studnicka, N. (2002). Archaeological scanning of Persepolis: using 3D laser scanning for mapping of ancient sites in Iran. GIM Int., 16 (6), 12 - 15.

Amann, M. C., Bosch, T., Lescure, M., Myllyla, R., and Rioux, M. (2001). Laser ranging: a critical review of usual techniques for distance measurement. Opt. Eng., 40 (1), 10 - 19.

Barber, D., Mills, J., and Bryan, P. (2001). Laser scanning and photogrammetry: 21st century metrology. Proc., 18th Int. Symposium of CIPA, Potsdam, Germany, 8.

Barber, D., Mills, J., and Bryan, P. (2003). Towards a standard specification for terrestrial laser scanning of cultural heritage. Proc., 19th Int. Symposium of CIPA, Antalya, Turkey, 6.

Boehler, W., Heinz, G., and Marbs, A. (2001). The potential of non-contact close range laser scanners for cultural heritage recording. Proc., 18th Int. Symposium of CIPA, Potsdam, Germany, 8.

Bornaz, L., Lingua, A., and Rinaudo, F. (2003). Terrestrial laser scanning: increasing automation for engineering and heritage applications. GIM Int., 17 (3), 12 - 15.

Caprioli, M., and Scognamiglio, A. (2003). Photogrammetry and laser scanning in surveying and 3D modelling of architectural heritage. Proc., FIG Working Week 2003, Paris, France, 7.

Cooper, M. A. R. (1982). Modern Theodolites and Levels, Granada Publishing Ltd., London, UK.

Fangi, G., Fiori, F., Gagliardini, G., and Malinverni, E. S. (2001). Fast and accurate close range 3D modelling by laser scanning system. Proc., 18th Int. Symposium of CIPA, Potsdam, Germany, 8.

Gordon, S. J., and Lichti, D. D. (2004). Terrestrial laser scanners with a narrow field of view: the effect on 3D resection solutions. Surv. Rev., In Press, 22 pages.
Guidi, G., Tucci, G., Beraldin, J.-A., Ciofi, S., Damato, V., Ostuni, D., Costantino, F., and El-Hakim, S. (2002). Multiscale archaeological survey based on the integration of 3D scanning and photogrammetry. Proc., CIPA WG 6 Int. Workshop on Scanning Cultural Heritage Recording, Corfu, Greece, 13 - 18.
Huising, E. J., and Pereira, L. M. G. (1998). Errors and accuracy estimates of laser data acquired by various laser scanning systems for topographic applications. ISPRS J. Photogramm., 53 (5), 245 - 261.
Kuang, S. (1996). Geodetic Network Analysis and Optimal Design: Concepts and Applications, Ann Arbor Press, Michigan, USA.
Marshall, G. F. (1985). Gaussian laser beam diameters. In: Laser Beam Scanning: Opto-Mechanical Devices, Systems, and Data Storage Optics, G. F. Marshall, ed., Marcel Dekker, Inc., New York, USA, 289 - 301.
Riegl (2001). LMS-210 Laser Mirror Scanner Technical Documentation and Users (sic) Instructions. Riegl Laser Measurement Systems.
Wehr, A., and Wiedemann, A. (2001). Fusion of photogrammetric and laser scanner data. Proc., 18th Int. Symposium of CIPA, Potsdam, Germany, 5.
Weichel, H., 1990. Laser Beam Propagation in the Atmosphere. SPIE Optical Engineering Press: Bellingham, WA.

BIOGRAPHICAL NOTES

Derek Lichti holds B.Tech. in Survey Engineering from Ryerson University, Toronto, Canada, and M.Sc. and Ph.D. degrees in Geomatics Engineering from the University of Calgary, Canada. His research interests are in terrestrial laser scanning and close-range photogrammetry. **Stuart Gordon** (B.Sc. (Hons.), Curtin) is a Ph.D. student with the Department of Spatial Sciences, Curtin University of Technology in Perth, Western Australia. His research focuses on terrestrial laser scanning.

CONTACTS

Dr. Derek Lichti and Stuart Gordon
Department of Spatial Sciences
Curtin University of Technology
GPO Box U1987
Perth, WA 6845
AUSTRALIA
Tel. + 61 8 9266 2691, +61 8 9266 3505
Fax + 61 8 9266 2703
Email: d.lichti@curtin.edu.au; s.gordon@curtin.edu.au
Web site: http://www.cage.curtin.edu.au/lascan/